

# Chapter 6

## Principles of Non-equilibrium Segregation

Although the basic goal of this book is to review fundamental aspects of equilibrium grain boundary segregation, it can also be reasonable to give brief information about the principles of non-equilibrium segregation, which occurs in many practical applications and plays an important role in mechanical properties of materials. In principle, this problem can be divided into two parts (a) kinetics of reaching equilibrium grain boundary segregation and (b) non-equilibrium segregation.

### 6.1 Kinetics of Grain Boundary Segregation

By annealing the sample containing grain boundaries, the diffusion processes run in the material thus redistributing the components to reduce the Gibbs energy of the system. This redistribution is time dependent and represents kinetics of reaching the final state – equilibrium redistribution of the solutes, that is equilibrium segregation. In principle, kinetics of grain boundary segregation can be considered from the point of view of semi-infinite solution of Fick equation applied to the system containing a grain boundary [19, 598]. In the following, we will use the description given by duPlessis and van Wyk [311].

#### 6.1.1 *Semi-infinite Solution of Fick Equation*

Let us suppose an ideal binary system containing a grain boundary between two semi-infinite bulk crystals in which the solute atoms diffuse towards the grain boundary. Such diffusion of solute  $I$  represented by the changes of its concentration  $X_I$  can be described by the second Fick law [311]

$$\left( \frac{\partial X_I}{\partial t} \right) = D_I \left( \frac{\partial^2 X_I}{\partial x^2} \right), \quad (6.1)$$

where  $D_I$  is the diffusion coefficient of solute  $I$ . The driving force of the diffusion is the concentration gradient, that is the flux of the atoms into the grain boundary region ( $x = 0$ ),

$$D_I \left( \frac{\partial X_I}{\partial x} \right)_{x=0} = \delta^\Phi \left( \frac{\partial X_I^\Phi}{\partial t} \right)_{x=0}. \quad (6.2)$$

In (6.2),  $\delta^\Phi$  is the thickness of the segregated layer. The grain boundary concentration  $X_I^\Phi$  is time-dependent and reaches the values  $X_I^{\Phi,\infty}$  at  $t \rightarrow \infty$  while  $X_I^\Phi = X_I^{\Phi,0}$  at  $t = 0$ . According to McLean [19],

$$X_I^{\Phi,0} = \frac{X_I^\Phi}{\beta_I^\Phi}, \quad (6.3)$$

where  $\beta_I^\Phi$  is the grain boundary enrichment factor (cf. (4.19)). The initial conditions for solution of (6.1) are  $X_I(x > 0, t = 0) = X_I^{\Phi,0}$ . The boundary condition is given by (6.3).

The diffusion equation (6.1) can be solved taking Laplace transform as [311]

$$\bar{X}_I = M \exp(-qx) + \frac{X_I^{\Phi,0}}{p}, \quad (6.4)$$

where  $q^2 = p/D$ .  $M$  is the constant, which can be determined as

$$M = \frac{(1 - \beta_I^\Phi) X_I^{\Phi,0} \delta^\Phi}{D_I q (\beta_I^\Phi q \delta^\Phi + 1)} \quad (6.5)$$

assuming the boundary condition

$$D_I \left( \frac{\partial \bar{X}_I}{\partial x} \right)_{x=0} = \beta_I^\Phi \delta^\Phi \left( p \bar{X}_I - \frac{X_I^{\Phi,0}}{p} \right). \quad (6.6)$$

Finally, we obtain an error function solution

$$X_I(x) = X_I^{\Phi,0} \left\{ 1 - \left( 1 - \frac{1}{\beta_I^\Phi} \right) \exp \left( \frac{x}{\beta_I^\Phi \delta^\Phi} + \frac{D_I t}{\beta_I^{\Phi^2} \delta^{\Phi^2}} \right) \operatorname{erfc} \left[ \frac{x}{2\sqrt{D_I t}} + \frac{\sqrt{D_I t}}{\beta_I^\Phi \delta^\Phi} \right] \right\} \quad (6.7)$$

which transforms for  $\beta_I^\Phi \gg 1$  to

$$X_I^\Phi = \beta_I^\Phi X_I \left[ 1 - \exp \left( \frac{D_I t}{\beta_I^{\Phi^2} \delta^{\Phi^2}} \right) \operatorname{erfc} \left( \frac{\sqrt{D_I t}}{\beta_I^\Phi \delta^\Phi} \right) \right] \quad (6.8)$$

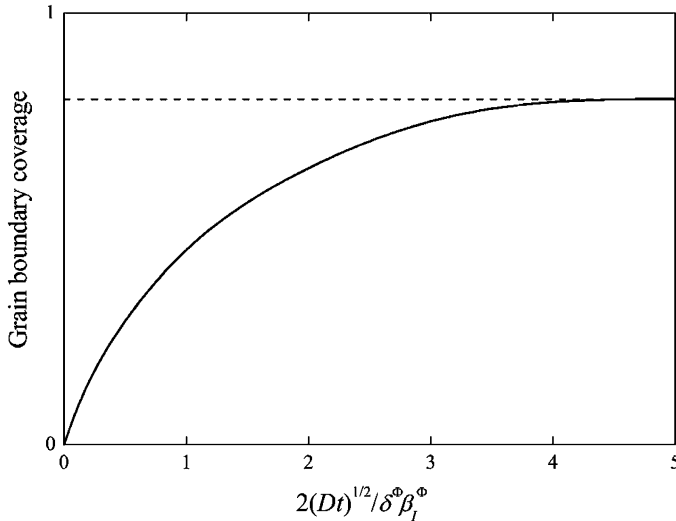


**Fig. 6.1** Time dependence of the kinetics of grain boundary segregation determined according to (6.8). According to [47]

or

$$\frac{X_{I,t}^\Phi - X_{I,t=0}^\Phi}{X_{I,t \rightarrow \infty}^\Phi - X_{I,t=0}^\Phi} = 1 - \exp \left( -\frac{D_I t}{\beta_I^\Phi \delta^\Phi} \right) \operatorname{erfc} \left( \frac{\sqrt{D_I t}}{\beta_I^\Phi \delta^\Phi} \right). \quad (6.9)$$

For short time  $t$ , a parabolic law is obeyed [311] (Fig. 6.1). It is supposed that the bulk concentration remains unchanged during the segregation process: As was shown above, this is valid for bicrystals and for polycrystalline materials of a wide spectrum of grain sizes albeit not for nanosized materials. Analytical solution of (6.9) assumes that the parameter  $\beta_I^\Phi$  does not change with the grain boundary concentration. This assumption is well fulfilled for low values of the grain boundary concentration.

The kinetics of the grain boundary segregation described above using the Langmuir–McLean segregation isotherm may be modified by application of more complex models of equilibrium grain boundary segregation such as Guttmann models (cf. Chap. 4). In this way, Seah [599] predicted the grain boundary segregation of impurities in steels for different times of annealing at various temperatures supposing mutual interaction between nickel and phosphorus. Theory of segregation kinetics in ternary systems including site competition and mutual interactions is shown in detail in [600] as well as other variations such as non-homogeneous initial distribution of solutes [601] or existence of surface phase transformations [415, 602].

A rather complex and unexpected behaviour was observed in case of sulphur segregation at (100) surfaces in an Fe–6at%Si alloy showing the influence of the sample history on the kinetics of the process [603]. These results evoked to modify the kinetic equations for accounting sulphide formation and pipe diffusion along

dislocations, and possible surface phase transitions for the case of higher coverage effects. Considering all these effects, the interfacial concentration of the segregated element represents the result of three contributions (a) bulk diffusion, (b) pipe diffusion along extended defects in the material (dislocations, grain boundaries) and (c) dislocation enrichment and precipitation. Thus,

$$X_{I,t}^\Phi = X_{I,t=0}^\Phi + X_{I,t} + X_{I,t}^d + X_{I,t}^{pv}, \quad (6.10)$$

where  $X_{I,t=0}^\Phi$  is the interfacial concentration of  $I$  at beginning of the process,  $X_{I,t}$  is the contribution following from bulk diffusion,  $X_{I,t}^d$  is the contribution of pipe diffusion and  $X_{I,t}^{pv}$  is the additional contribution to interfacial segregation due to the solute enrichment of dislocations. The complete kinetics of surface segregation is then expressed as

$$\begin{aligned} X_{I,t}^\Phi - X_{I,t=0}^\Phi &= \frac{2X_{I,t=0}}{\delta^\Phi X_{I,t \rightarrow \infty}^\Phi} \sqrt{\frac{D_I t}{\pi}} + \frac{2d_d X_{I,t=0}^d}{\delta^\Phi X_{I,t \rightarrow \infty}^\Phi} \sqrt{\frac{D_I^d t}{\pi}} \\ &+ \frac{4d_d \pi (X_{I,t=0} - X_I^*)}{3\delta^\Phi X_{I,t \rightarrow \infty}^\Phi} \frac{D_I^d t}{a^2 \ln(L/a)} \sqrt{\frac{D_I^d t}{\pi}}, \end{aligned} \quad (6.11)$$

where  $d_d$  is the dislocation density related to the total amount of the atomic sites,  $2L$  is the average distance between precipitates at the dislocations,  $2a$  is the inner width of the dislocation core, and  $X_I^*$  is the solubility limit of the solute. Despite some simplification, this model was successfully used to interpret the kinetics of surface segregation in the above mentioned Fe–6at%Si alloy [603].

### 6.1.2 Layer-by-Layer Model (Model of Hofmann and Erlewein)

Hofmann and Erlewein [604] supposed that the course of the potential (Gibbs) energy in direction perpendicular to the interface is periodic with the barrier  $\Delta G_D$  in the bulk. In the interface layer 1, the minimum is lower by  $\Delta G(\Phi)$  (Fig. 6.2). During diffusion, the atoms jump from layer to layer and overcome the barriers. Supposing the fluxes between the layers,  $J_{i,j}$ , with  $j = i \pm 1$ , we can solve the Fick laws. The first Fick law

$$J_x = -D_{I,x} \frac{\partial X_I}{\partial x} \quad (6.12)$$

describes the flux through the plane in distance  $x$  from the interface ( $x = 0$ ) in one-dimensional case. For small changes in concentration, we can approximate for cubic structure  $\partial x = a$ , where  $a$  is the lattice parameter and  $\partial X_I = X_{I(i+1)} - X_{I(i)}$  is the difference in concentrations of two neighbour atomic layers,

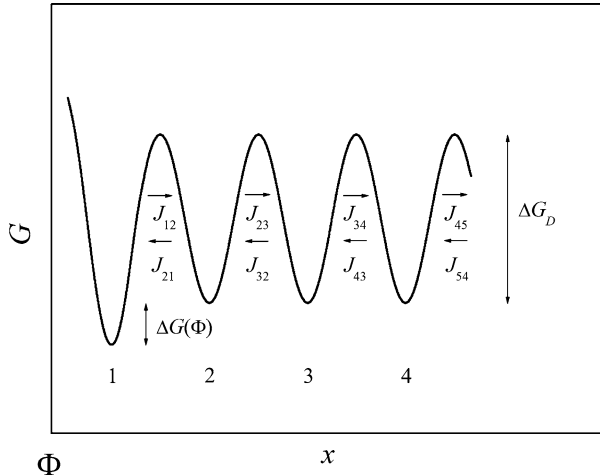


**Fig. 6.2** Schematic depiction of the layer-by-layer course of the potential Gibbs energy in direction  $x$  perpendicular to the interface  $\Phi$ . According to [604]

$$J_{i+1,i} = -D_{I,i+1,i} \frac{X_{I+1} - X_{I,i}}{a}. \quad (6.13)$$

Supposing

$$D_I = D_{0,I} \exp\left(-\frac{Q}{RT}\right) = a^2 v \exp\left(-\frac{Q}{RT}\right), \quad (6.14)$$

the evaluation of (6.13) for individual layers provides us with

$$J_{12} = \frac{X_{I,1} W_{12} v_1}{a^2} \exp\left(-\frac{\Delta G_D + \Delta G(\Phi)}{RT}\right), \quad (6.15)$$

$$J_{21} = \frac{X_{I,2} W_{21} v_2}{a^2} \exp\left(-\frac{\Delta G_D}{RT}\right), \quad (6.16)$$

and

$$J_{i,i+1} = \frac{X_{I,i} W_{i,i+1} v_i}{a^2} \exp\left(-\frac{\Delta G_D}{RT}\right), \quad (6.17)$$

etc., where  $v_i$  is the frequency of atomic jumps in layer  $i$  and  $W_{i,i+1}$  is the jump probability. In the bulk, the probability of the jumps is

$$W_{i,i+1} = 1 - X_{I,i \pm 1}, \quad (6.18)$$

while in vicinity of the interface layer

$$W_{21} = \left(1 - \frac{X_{I,1}}{X_I^\Phi}\right)^{X_I^\Phi}, \quad (6.19)$$

where  $X_I^\Phi$  is the equilibrium interfacial concentration at this temperature.

The rate of the concentration changes can be expressed using the second Fick law

$$\frac{dX_{I,1}}{dt} = a^2(J_{21} - J_{12}). \quad (6.20)$$

Thus [604]

$$\frac{dX_{I,1}}{dt} = \frac{D_I}{a^2} \left[ W_{21}X_{I,2} - W_{12}X_{I,1}\exp\left(-\frac{\Delta G(\Phi)}{RT}\right) \right] \quad (6.21)$$

and

$$\begin{aligned} \frac{dX_{I,i}}{dt} &= a^2(J_{i-1,i} + J_{i+1,i} - J_{i,i-1} - J_{i,i+1}) \\ &= \frac{D_I}{a^2} [W_{i-1,i}X_{I,i-1} + W_{i+1,i}X_{i+1} - W_{i,i-1}X_{I,i} - W_{i,i+1}X_{I,i}]. \end{aligned} \quad (6.22)$$

Numerical solution of the above equations for high values of  $\Delta G(\Phi)$  results in parabolic dependence [604]. Model of Hofmann and Erlewein was extended for ternary alloys by Boudjemaa and Moser [605].

### 6.1.3 Model of Limited Reaction Rates

In cases when the bulk diffusion is faster than that at interface (e.g. in case of diffusion of carbon in tungsten [606]) the flow of solutes to the interface is constant and the rate of segregation is controlled by concentration difference at the interface between the equilibrium and actual concentrations,  $X_{I,\text{eq}}^\Phi$  and  $X_I^\Phi(t)$ , respectively,

$$\frac{dX_I}{dt} = k \left( X_{I,\text{eq}}^\Phi - X_I^\Phi(t) \right), \quad (6.23)$$

where  $k$  is the reaction rate constant. Integration of (6.23) results in

$$X_I^\Phi(t) = X_{I,\text{eq}}^\Phi [1 - \exp(-kt)]. \quad (6.24)$$

## 6.2 Non-equilibrium Segregation

During some processes in which the non-equilibrium character prevails, additional (non-equilibrium) point defects may be introduced into the materials containing the grain boundaries. As a result of the interaction of the solute atoms with these point defects the chemical composition of grain boundaries may be substantially changed as compared to equilibrium segregation. This effect is called *non-equilibrium segregation*. The mechanism of the non-equilibrium segregation

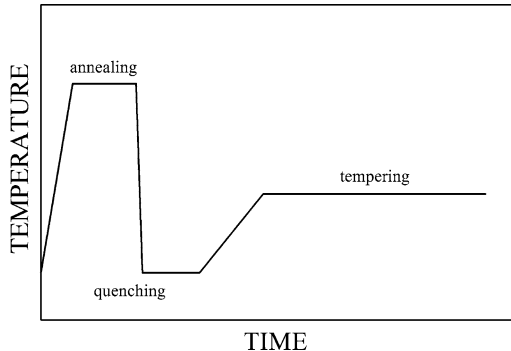


**Fig. 6.3** Schematic depiction of thermal treatment needed to produce non-equilibrium segregation. According to [18]

consists in formation of impurity–vacancy complexes in the volume [18, 47]. There are three basic types of non-equilibrium segregation (a) thermally induced segregation, (b) radiation-induced segregation and (c) stress-induced segregation [47]. Additionally, we may also consider the segregation at moving grain boundaries as non-equilibrium segregation.

### 6.2.1 Thermally Induced Segregation

One of the processes producing additional point defects is quenching after a heat treatment. In this way, the vacancy supersaturation occurs. During subsequent heating at moderate temperatures, (Fig. 6.3) the concentration of non-equilibrium vacancies changes and redistributes region-to-region in the microstructure. Because the interfaces are efficient sinks for vacancies, their concentration in vicinity of the grain boundaries is quickly reduced while their supersaturation in the matrix preserves. Consequently, a concentration gradient of vacancies establishes between the crystal volume and the grain boundaries and the vacancies should move towards the grain boundaries. However, the vacancies in matrix – mainly in case when a substantial misfit between solute and solvent atoms exists – form the impurity–vacancy complexes, which drag this movement but help to bring the impurity atoms close to the boundary. Consequently, an enrichment of the regions in vicinity of the grain boundaries occurs on the scale of several nanometres. This is not an equilibrium state. Indeed, a prolonged tempering can erase the effect of non-equilibrium segregation [18, 47]. Such processes were firstly observed about 50 years ago [607, 608].

According to Bercovici et al. [609], the number of complexes  $N_c$  reaching the grain boundary during quenching is

$$N_c = \int_0^{t_f} x(t) \left( dX_c - dX_c^\Phi \right), \quad (6.25)$$

where  $x(t)$  is the distance of impurity diffusion in time  $t$ ,  $X_c^\Phi$  and  $X_c$  are the concentrations of the complexes at the grain boundary and in the grains, respectively, and  $t_f$  is the time of quenching. This model is physically realistic but is limited to numerical solution of the integral.

In the model of Doig and Flewitt [610], the error function solution of the Fick equation was used to analyse the vacancy concentration profile in the grain boundary region for a series of small time intervals of quenching,  $\Delta t$ , as

$$\frac{X_{V,x} - X_{V,\Delta t}^\Phi}{X_{V,t=0}^\Phi - X_{V,\Delta t}^\Phi} = \operatorname{erfc} \left( \frac{x}{2\sqrt{D_V \Delta t}} \right), \quad (6.26)$$

where  $X_{V,x}$  is the vacancy concentration at a distance  $x$  from the boundary,  $X_{V,\Delta t}^\Phi$  is the vacancy concentration at the grain boundary at the quenching temperature for the quenching time  $\Delta t$ ,  $X_{V,\Delta t=0}^\Phi$  is the vacancy concentration at the grain boundary at the quenching temperature at zero time (= volume concentration of vacancies) and  $D_V$  is the vacancy self-diffusivity in matrix [18]. The temperature  $T_n$  reached during the cooling over a period  $\Delta t$ , can be estimated according to

$$T_n = T_s \exp(-\varphi_n \Delta t) \quad (6.27)$$

with  $T_s$  and  $\varphi_n$  being the starting temperature and the number of the time step. For each temperature and time interval, a series of vacancy concentration profiles can be obtained. The spatial extent of the vacancy concentration profile,  $x_n$ , is expressed as

$$x_n = 2\sqrt{D_{v(n)} \Delta t}. \quad (6.28)$$

The final situation is then represented by an envelope of the curves [18, 47, 610].

A general and simple model of non-equilibrium segregation was also developed by Faulkner [611]. The non-equilibrium grain boundary enrichment ratio  $\beta_I^\Phi$  (4.19) is predicted as

$$\beta_I^\Phi = \frac{X_I^\Phi}{X_I} = \exp \left( \frac{E_c^b - E_V^f}{k T_i} - \frac{E_c^b - E_V^f}{k T_{0.5T_m}} \right) \frac{E_c^b}{E_V^f}. \quad (6.29)$$

In (6.29),  $E_c^b$  and  $E_V^f$  are the binding energy of the complex and the vacancy formation energy, respectively, and  $T_i$  and  $T_m$  are the absolute starting temperature and absolute melting temperature of the material. For simplicity, all calculation is done at  $T_i$ . An effective time of quenching is then

$$t = \frac{K^* k T_i^2}{\varphi E_a}, \quad (6.30)$$

where  $E_a$  is the effective activation energy for bulk self-diffusion and impurity diffusion and  $K^* \approx 0.01$  is a constant. This model additionally admits existence

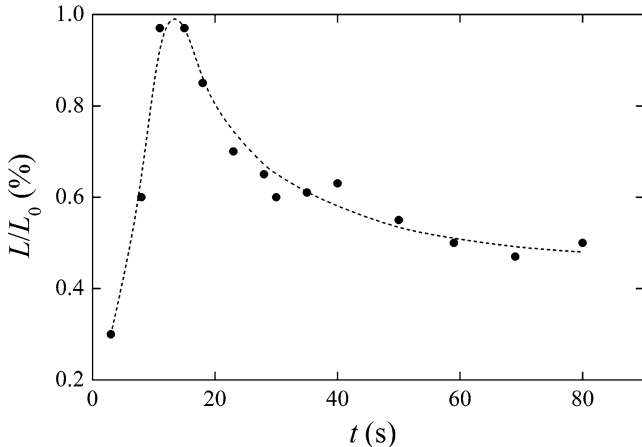


**Fig. 6.4** Time dependence of the ratio  $L/L_0$  of an Fe–30%Ni(B) alloy hold at 1,050°C after isothermal annealing at 1,250°C for 0.5 h followed by quenching to ice-water.  $L_0$  is the total length of the grain boundaries in a unit cross-section area and  $L$  is the length of the grain boundaries in the same area. According to [613]

of the critical time  $t_c$  of slow quenching or fast heating after that the equilibrium segregation establishes. The critical time is given by

$$t_c = \frac{d^2 \ln(D_c/D_l)}{4\delta(D_c - D_l)}, \quad (6.31)$$

where  $d$  is the grain size,  $D_c$  and  $D_l$  are the complex and the impurity bulk diffusivities, respectively, and  $\delta \approx 0.05$  is a constant [18, 47, 611, 612]. Existence of  $t_c$  was first experimentally confirmed in case of boron segregation in an Fe–30%Ni base alloy [613] (Fig. 6.4) and further observed for boron segregation in a Mn–Mo–B steel [614] and in Fe–40%Al intermetallics [128]. Due to the temperature dependence of the diffusion coefficients, the rate of grain boundary segregation increases with increasing temperature and the critical time is shorter [615]. As a result, a temperature should exist at which the non-equilibrium segregation reaches maximum for an alloy quenched from a chosen annealing temperature (Fig. 6.5) [374, 615, 616].

Maier and Faulkner [617] point out that the final segregation level at the grain boundary may also be affected by the history of the sample. They document this statement, for example of the weld chemistry in phosphorus-containing Mn–C steel. The final segregation amount is the sum of each single step. Phosphorus segregation, which is primarily controlled by equilibrium segregation, depends on concentration of alloying elements and on temperature, but is independent of the microstructure and the thermal history. In fact, its segregation is governed by the final annealing conditions. On the other hand, manganese segregation is dependent

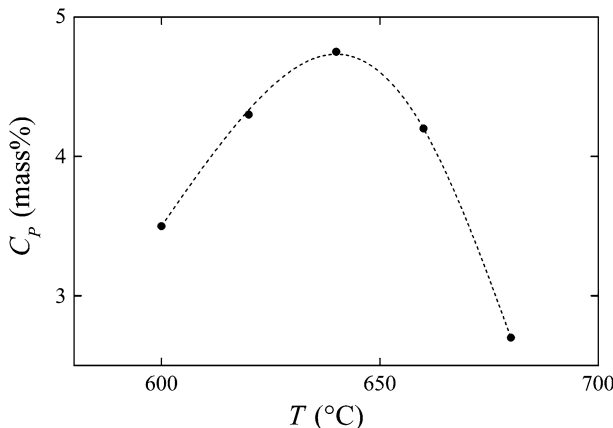


**Fig. 6.5** Grain boundary concentrations of phosphorus in steel aged at 600, 620, 640, 660, and 680°C for 70 h after quenching from a temperature of 1,050°C. According to [615]

on the microstructure (grain size) and the welding temperature, but independent of presence of the additional elements and only slightly dependent on the service temperature.

### 6.2.2 Radiation-Induced Segregation

Another source of production of point defects is an irradiation of the sample, usually by neutrons. The major difference between this source and production of non-equilibrium point defects by thermal shocks is that interstitials also affect the segregation process. In the irradiated materials, a stronger binding occurs between interstitials and impurity atoms than with vacancies [18, 47]. Besides the interstitial–impurity binding energy, the other main factors controlling the magnitude of the radiation-induced segregation are the relative diffusion rates of the free impurities and the impurities forming complexes in the matrix. Let us note that strong interaction between the interstitial and impurity atoms only occurs in case of a negative misfit, that is when the impurity atom is smaller than the matrix atom. This contrasts with interaction of vacancies with impurity atoms that form complexes despite of the character of the misfit [18, 47]. Typical concentration profiles of individual mechanisms of non-equilibrium segregation are schematically depicted in Fig. 6.6.

To describe the radiation-induced segregation, the rate theory has also been applied. Generally, the total concentrations of vacancies,  $X_V$ , interstitials,  $X_{\text{int}}$ , and solute atoms,  $X_I$ , are given as

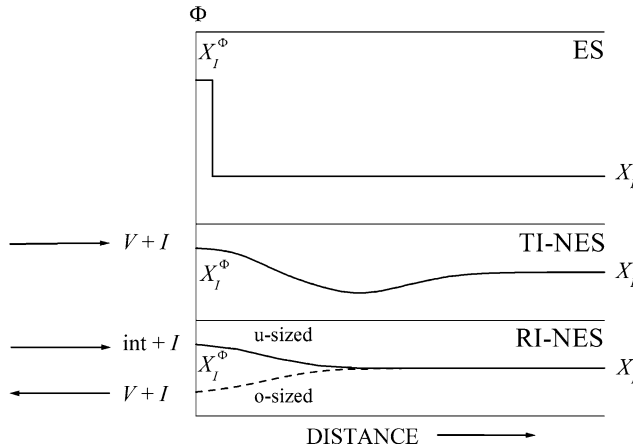


**Fig. 6.6** Schematic representation of concentration profiles of a solute in cases of thermally and radiation-induced non-equilibrium segregation. For comparison, the same representation for the equilibrium segregation is also shown. *ES* equilibrium segregation, *TI-NES* thermally induced non-equilibrium segregation, *RI-NES* radiation-induced non-equilibrium segregation, *u-sized* undersized, *o-sized* oversized solutes  $I$ ,  $V$  and  $int$  vacancies and interstitials, respectively

$$\left( \frac{\partial X_V}{\partial t} \right) = K - \alpha X_{int} X_V - L_V - \nabla I_V, \quad (6.32)$$

$$\left( \frac{\partial X_{int}}{\partial t} \right) = K - \alpha X_{int} X_V - L_{int} - \nabla I_{int}, \quad (6.33)$$

$$\left( \frac{\partial X_I}{\partial t} \right) = -\nabla I_I, \quad (6.34)$$

where  $I_V$ ,  $I_{int}$  and  $I_I$  are the fluxes of vacancies, interstitials and solute atoms, respectively,  $K$  is the production rate for vacancies and interstitials,  $\nabla$  is the recombination coefficient and  $L_V$  and  $L_{int}$  are the respective dose rates for vacancies and interstitials to dislocations and/or grain boundary sinks. Taking into account that some of the point defects can disappear within the material, the boundary condition  $I_V = I_{int} = I_I$  should be fulfilled at the grain boundary, the thickness of the boundary is spread to about ten atomic spacings, the fluxes of the point defects ( $pd = V, int$ ) from the surface to the material are given as

$$I_{pd} = D_{pd}^{\text{eff}} \left( X_{pd} - X_{pd}^s \right) / \mu_{pd} + N_{pd} v, \quad (6.35)$$

where  $X_{pd}^s$  is the equilibrium concentration of  $pd$  at the surface,  $\mu_{pd}$  is the rate limiting parameter for the absorption of point defects  $pd$  and  $v$  is the velocity of the receding surface due to the sputtering.

In another approach, the variables such as the diffusivities of the solute and the interstitial–solute complex, grain size, dislocation density, neutron dose, dose rate, interstitial formation, binding energies of the guest atoms with either the solute or

the impurity atoms and temperature are considered. The maximum grain boundary segregation,  $X_{I,\max}^\Phi$ , is given as [47, 618–620]

$$X_{I,\max}^\Phi = X_I \frac{E_I^b}{E_I^f} \left[ 1 + \frac{B_R G^*}{KD_{\text{int}} k_d^2} \exp\left(\frac{E_I^f}{kT}\right) \right], \quad (6.36)$$

where  $E_I^b$  and  $E_I^f$  are the solute–interstitial binding energy and the interstitial formation energy, respectively,  $D_{\text{int}}$  is the interstitial diffusivity,  $K$  is a geometrical constant,  $G^*$  is the production rate of the point defects that is proportional to the neutron dose rate,  $B_R$  is the dose rate correction factor and  $k_d$  is the sink strength of the grain volume for interstitials,

$$k_d = \sqrt{K_Z \rho_{\text{disl}}} \times \sqrt{6/d + \sqrt{K_Z \rho_{\text{disl}}}}. \quad (6.37)$$

In (6.37),  $\rho_{\text{disl}}$  is the dislocation density,  $K_Z$  is a bias parameter defining preferred interaction between interstitials and dislocations compared with vacancies and dislocations and  $d$  is the grain size [47]. Similarly to the thermally induced segregation (6.31), there exists a critical time  $t_c$  of the slow quenching or fast heating after that the equilibrium segregation establishes. The critical time is given by [47]

$$t_c = \frac{\delta d^2 \ln(D_{\text{int}}/D_I)}{4(D_{\text{int}} - D_I)}. \quad (6.38)$$

Frequently, the radiation-induced segregation is explained on basis of the inverse Kirkendall mechanism (e.g. [621–623]). Similarly to equilibrium segregation, anisotropy of non-equilibrium segregation is also observed. For example, the  $\Sigma = 3$  twin grain boundaries in 304 grade stainless steel were found to be resistant to solute segregation, while the level of chromium segregation increases with increasing value of  $\Sigma$  [622]. Generally, the oversized solute atoms suppress the radiation-induced segregation at grain boundaries in austenitic stainless steels. The mechanisms of this effect may be different. Platinum reduces the diffusion rates of the point defects and influences subsequent defects aggregation, while hafnium increases the recombination rate of point defects possibly through formation of additive-vacancy complexes [624]. The flow of the undersized nickel solute toward the grain boundary may be facilitated by the grain boundary migration [625]. In nickel, however, the segregation of oversized atoms – manganese, palladium and niobium – is enhanced by interaction with interstitials [626].

A model of radiation-induced segregation and migration based on diffusion and reaction rate equations was proposed by Sakaguchi et al. [627]. The model considers the rearrangement of the grain boundary plane during its migration induced by radiation. The non-equilibrium point defects induced by this process, their recombination, annihilation and rearrangement are taken into account. The calculations indicate a progressive expansion of the chromium-depleted zone along the grain boundary during its migration. The results of the calculations are in good agreement with experimental data on the behaviour of an austenitic stainless steel obtained

by the same authors. It was also shown that presence of third elements and their segregation suppresses the chromium segregation level and width [628].

A possible mechanism of the chromium segregation depends on whether it is oversized or undersized relatively to other solutes and in dependence on its concentration and electronic and/or magnetic effects. If it is undersized, the complexes chromium–self-interstitial iron may be preferentially formed and chromium atoms will be solute dragged towards grain boundaries. The oversized chromium atoms will drift away from grain boundaries due to a negative binding solute-drag mechanism [629]. Chromium segregates, therefore, during radiation of Fe–13Cr–1Si, HT–9, 12CrMoVNb, HCM12A and T91 steels, while it is depleted from the boundaries in high chromium ferritic/martensitic and austentic steels F82H, E911, 13Cr2MoVNbB, 13Cr2Mo+TiO, Fe–5Cr, Fe–13Cr–1Ti [623]. Similar effect in suppressing intergranular stress corrosion cracking have zirconium and – in some extent – also hafnium [630], platinum and titanium [631]. Irradiation of 304 austenitic stainless steel evokes the grain boundary segregation of nickel and the depletion of the grain boundaries by chromium and manganese. This results in reduction of intergranular cohesion of this material [632].

### 6.2.3 Stress-Induced Segregation

Plastic deformation induces formation of non-equilibrium vacancies in alloys. The supersaturated vacancies can interact with solute atoms and create supersaturated vacancy–solute complexes thus inducing non-equilibrium grain boundary segregation of a solute via complex diffusion to the grain boundary [633]. However, the number of studies of grain boundary segregation during plastic deformation has been rare till now.

Annihilation of vacancies at grain boundaries results in reduction of their concentration and in its approaching to the equilibrium value. As the vacancy concentration in the grain volume remains non-equilibrium since there are no vacancy sinks, the vacancy concentration gradient is formed between the grain interior and the boundary. As a consequence, there also exists the concentration gradient of the vacancy–solute complexes, and these complexes diffuse to the grain boundary.

It is assumed that during high temperature plastic deformation, the annihilation of vacancies within the grains is diffusion controlled and takes place predominantly at dislocations that are the sinks of vacancies. The concentration of non-equilibrium vacancies in the steady-state,  $X_{\text{se}}$ , at a given strain rate,  $\dot{\varepsilon}$ , can be expressed as [620]

$$X_{\text{se}} = \frac{\kappa^2 \mu^2 \Omega_0}{D_V} A^{1/n} \exp\left(-\frac{Q_{\text{def}}}{nkT}\right) \times \left[ \frac{\chi b^2}{Q_f^V} \dot{\varepsilon}^{(1-1/n)} + \frac{\xi X_j}{4b} A^{1/n} \exp\left(-\frac{Q_{\text{def}}}{nkT}\right) \dot{\varepsilon}^{(1-2/n)} \right], \quad (6.39)$$

where  $\kappa$  is the structural parameter describing the distribution of dislocations, (for homogeneous distribution,  $\kappa = 1$ ),  $\mu$  is the shear modulus,  $\Omega_0$  is the atomic volume,

$D_V$  is the vacancy diffusivity,  $Q_f^V$  is the energy of vacancy formation,  $A$  and  $n$  are constants,  $Q_{\text{def}}$  is the apparent activation energy for deformation,  $b$  is the Burgers vector of the dislocations,  $X_j$  is the concentration of thermal jogs,  $\chi$  is the constant associated with the mechanical production of jogs, and  $\xi$  is the parameter depicting the neutralisation effect produced by the presence of vacancy emitting and vacancy absorbing jogs.  $X_j$  can be expressed as

$$X_j = \exp\left(-\frac{E_j}{kT}\right), \quad (6.40)$$

where  $E_j$  is the energy of jog formation. The vacancy diffusivity in pure metals is given by

$$D_V = D_{V0} \exp\left(-\frac{Q_m^V}{kT}\right) \quad (6.41)$$

where  $Q_m^V$  and  $D_{V0}$  are the vacancy migration energy and the pre-exponential factor for vacancy diffusion, respectively. In case of alloys the vacancy may migrate by exchanging the position either with the host atom or with the solute atom. Therefore, (6.41) only represents an estimate which is reasonable for dilute alloys where the vacancy migration preferentially realises via exchange with the host atoms [634].

The concentration of vacancies in the matrix in a steady state,  $X_{Vs}$ , is equal to the sum of the concentrations of non-equilibrium vacancies,  $X_{se}$ , and the equilibrium vacancy concentration,  $X_{th}$ , which can be expressed for a pure metal as

$$X_{th} = B \exp\left(-\frac{Q_f^V}{kT}\right), \quad (6.42)$$

where  $B$  is a constant. In case of an alloy, (6.42) is again only an estimate, although well acceptable for dilute alloys as discussed above for (6.41).

The concentration of vacancy–solute complexes,  $X_{IV}$ , is given by [633, 634]

$$X_{IV} = m X_I X_V \exp\left(\frac{Q_{IV}}{kT}\right), \quad (6.43)$$

where  $m$  is a constant,  $X_V$  is the vacancy concentration, and  $Q_{IV}$  is the binding energy between a vacancy and a solute atom. In the regions far away from the grain boundary,  $X_V = X_{VI}$ . Assuming that  $X_I$  is invariable,  $X_V = X_{th}$  in vicinity of the grain boundaries, maximum grain boundary concentration of solute  $I$ ,  $X_{I,\max}^\Phi$ , is [634]

$$\begin{aligned} X_{I,\max}^\Phi &= X_I^\Phi + X_I \frac{Q_{IV}}{Q_f^V} \left\{ 1 + \frac{\kappa^2 \mu^2 \Omega_0 A^{1/n}}{D_V B} \exp\left(-\frac{Q_{\text{def}}}{nkT}\right) \right. \\ &\quad \times \left[ \frac{\chi b^2}{Q_f^V} \dot{\varepsilon}^{(1-1/n)} + \frac{\xi X_j A^{1/n}}{4b} \exp\left(-\frac{Q_{\text{def}}}{nkT}\right) \dot{\varepsilon}^{(1-2/n)} \right] \times \exp\left(\frac{Q_f^V}{nkT}\right) \left. \right\}. \end{aligned} \quad (6.44)$$

$X_{I,\max}^\Phi$  can be obtained from the expressions for the kinetics of segregation (6.38) and (6.39).

A significant amount of vacancies can also be produced during creeping a material at temperatures above  $0.4T_m$ . In such processes, the dimension of the material is changed to accommodate the stresses by the emission of vacancies from grain boundaries in a transverse direction to the direction of the stress. Simultaneously, there can move the over- or undersized solute or impurity atoms. As considered previously, vacancy–solute complexes may occur and if their binding energy is advantageous, they may drag the solute atoms moving to grain boundaries [47]. The effect of applied stress can be divided into two mechanisms (a) the reduction of grain boundary segregation due to modified diffusion rate of solute atoms in grain volume, and (b) the reduction of the absorption ability of grain boundaries for the solute atoms due to change of the grain boundary free energy [620]. Another model proposes production of non-equilibrium vacancies by non-conservative motion of jogs on screw dislocations at low temperatures [635]. Solute segregation is closely connected with growth of the cracks under stress and many models in this field were developed to describe the cracking of the material [47]. This consideration is out of scope of this book.

#### 6.2.4 Grain Boundary Segregation and Migration

The dragging effect of segregated solutes on the grain boundary migration is notoriously known (cf. [48]). The atmosphere of the solute atoms tends to move with migrating grain boundary, however, the velocity of its diffusion is substantially lower than the rate of the grain boundary migration as the latter process is diffusionless. The interaction of the slowly diffusing solutes with the boundary results in a dragging force. The rate  $v$  of the boundary motion is slowed down

$$v = m(P - P_v(v)), \quad (6.45)$$

where  $P$  and  $P_v(v)$  are the driving force of the grain boundary migration and the dragging term, respectively. Increasing bulk concentration of the solute has a more pronounced effect to the general grain boundaries as compared to the special ones [636]. The strongest effect of the solute segregation to the anisotropy of grain boundary migration is probably observed in case of very pure materials. In absolutely pure metals, it is supposed that special grain boundaries will migrate hardly because there is a high activation barrier to change their orientation by curving, which is necessary for the boundary migration. On the other hand, general boundaries should move rather simply in pure metals. Due to increasing concentration of impurities, the general grain boundaries are more strongly segregated than the special grain boundaries, and therefore, the rate of their motion decreases. At a suitable bulk concentration of impurities, the rate of migration of all boundaries is nearly the same. If the bulk concentration of impurities further increases, a reversed effect appears: Special

grain boundaries can migrate more quickly than general ones. After saturation of the grain boundaries by the segregated impurities, the migration of all boundaries is again equalised [48].

It is obvious that during the grain boundary migration, the concentration distribution of the solute atoms becomes asymmetrical. Supposing migration of a planar grain boundary in  $x$ -direction with constant velocity  $v$ , the grain boundary concentration of solute  $I$ ,  $X_I^\Phi$ , can be described as a unidirectional case [48]

$$\frac{\partial X_I(x, t)}{\partial t} = D_I \frac{\partial^2 X_I(x, t)}{\partial x^2} + \frac{\partial}{\partial x} \left( \frac{D_I X_I(x, t)}{kT} \frac{dU}{dx} \right), \quad (6.46)$$

where  $D_I$  is the volume diffusivity and  $X_I(x, t) = X_I$  for  $x \rightarrow \pm\infty$ . The co-ordinate system is supposed to have its origin located in the boundary plane, so moving with the grain boundary. The solute distribution across the migrating grain boundary can reach a steady state so that  $\partial X_I(x, t)/\partial t = 0$ . To simplify the problem, Gottstein and Shvindlerman [48] assume

$$U(x) = 0 \quad \text{for } |x| \geq a \quad \text{and} \quad U(x) = H_0 \quad \text{for } |x| \leq a. \quad (6.47)$$

Therefore,  $dU/dx = 0$  except the discontinuities at  $x = \pm a$ . Supposing the Galilei transformation  $x = x' - vt$ , the diffusion equation in the moving co-ordinate system reduces to

$$\frac{\partial X_I(x, t)}{\partial t} = D_I \frac{\partial^2 X_I(x, t)}{\partial x^2} + v \frac{\partial X_I(x, t)}{\partial x} \quad (6.48)$$

for  $x \neq \pm a$ . The solution of this equation provides

$$X_I(x, t) = X_I + X_I(a) \exp\left(-\frac{vx}{D_I}\right). \quad (6.49)$$

The concentration behind the grain boundary is  $X_I(x, t) = X_I$  for  $x \rightarrow -\infty$ . The concentration of the solute in front of the boundary is

$$(X_I)_F = X_I + (X_I(a) - X_I) \exp\left(-\frac{vx}{D_I}\right). \quad (6.50)$$

Let us repeat that the potential  $U$  is discontinuous for  $x = \pm a$ . Therefore, the constant  $X_I^\Phi$  as well as the concentration distribution cannot be determined in closed form [48]. Supposing the steady state is reached during the migration, the diffusion flux is constant at any  $x$ , that is  $J_X = vX_I$ . Assuming the thickness of the grain boundary is comparable to a single atomic layer in the bulk, the flux through the interface plane between the grain boundary  $\Phi$  and the bulk in front of the grain boundary ( $x = +a$ ) is

$$X_I^\Phi \frac{D_I}{b} \exp\left(-\frac{H_0}{kT}\right) - X_I(a) \frac{D_I}{b} - vX_I(a) = -vX_I, \quad (6.51)$$

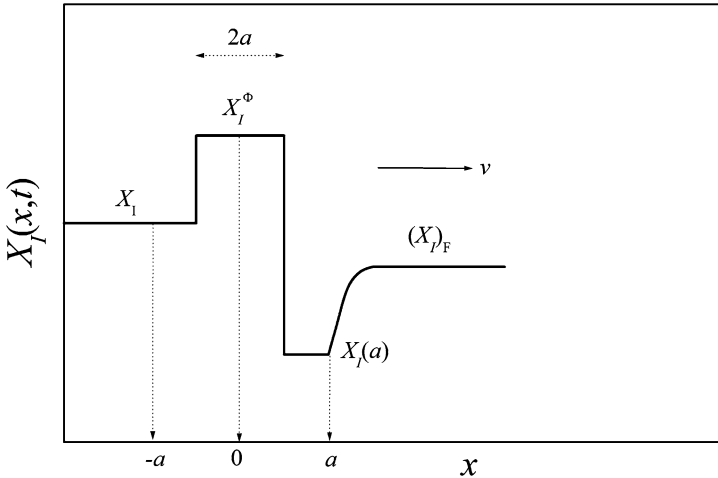


**Fig. 6.7** Model of a concentration distribution of the solutes in the vicinity of a grain boundary migrating in a steady state. According to [48]

where  $b$  is the atom diameter. The flux through the interface plane between the boundary  $\Phi$  and the bulk ( $x = -a$ ) is (Fig. 6.7)

$$X_I \frac{D_I}{b} - X_I^\Phi \frac{D_I}{b} \exp\left(-\frac{H_0}{kT}\right) - v X_I^\Phi = -v X_I. \quad (6.52)$$

Since the first two terms of (6.51) describe the diffusion fluxes through the mentioned interface plane, we can write them as

$$X_I^\Phi v \exp\left(-\frac{H_0 + H_D}{kT}\right) - X_I(a) v \exp\left(-\frac{H_D}{kT}\right) \quad (6.53)$$

with  $H_D$  representing the activation enthalpy of volume diffusion. Equation (6.52) can be treated similarly. Then

$$X_I^\Phi = X_I \frac{D_I + bv}{D_I \exp(-H_0/kT) + bv} \geq X_I \quad (6.54)$$

and

$$X_I = 1 - \frac{D_I bv(1 - \exp(-H_0/kT))}{(D_I + bv)(D_I \exp(H_0/kT) + bv)}. \quad (6.55)$$

Corresponding concentration profile is shown in Fig. 6.7.

Similar result was obtained by the phase field model of Cha et al. [637]. They constructed a movable abstract boundary between two grains with rapid diffusion within it while the diffusion in the grain is neglected. Considering two variables, the solute concentration and the phase field,  $f$  ( $f = 1$  for one grain and  $f = 0$  in the

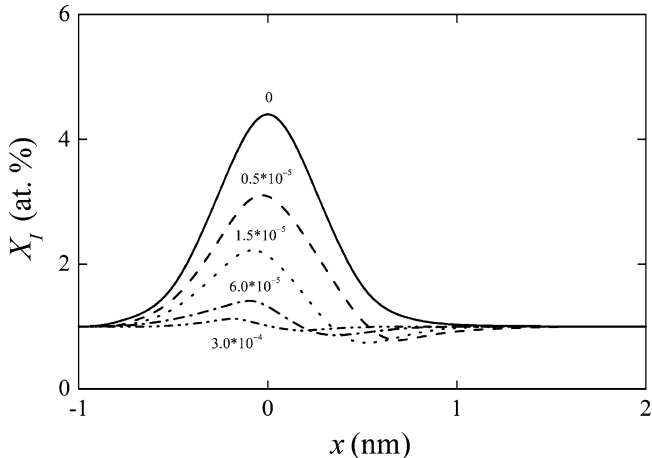


**Fig. 6.8** Concentration profiles for various velocities: equilibrium segregation (no migration,  $v = 0$ ): full line, low velocity: dashed line, velocity of the maximum drag: dotted line, the inflection in the drag–velocity curve: dashed-dotted line, high velocity: dashed-dotted-dotted line. According to [637]

other grain). The interfacial region is a mixture of the grain and the grain boundary with different concentrations but with the same chemical potential. The concentration profile across the grain boundary in dependence on its migration velocity is shown in Fig. 6.8. Similar concentration distribution of the solute around the migrating grain boundary was found in simulations of kinetics of grain boundary migration and prediction of solute-drag-effect induced abnormal grain growth [638].

Simulations performed on basis of the phase field model showed that particularly in strongly segregating systems the concentration of a solute at the moving grain boundary can increase with increasing the migration velocity to such an extent that the level of segregation can be higher than that in equilibrium. The drag force of the solute segregation also causes deviations of the relationship between the migration rate and the curvature from linearity [639].

Similar results were obtained by means of a self-consistent continuum model of grain boundary segregation and segregation transition based on gradient thermodynamics and its relations to the discrete lattice model. This model stresses out the role of some distinctive terms that were ignored in previous models such as concentration gradient, spatial variation of the gradient-energy coefficient and concentration dependence of solute–grain boundary interactions and can predict the segregation transition (i.e. the transition from low to high segregation) that takes place with changing temperature, bulk composition and/or grain boundary velocity. This transition, which is first-order with a hysteresis, is responsible for the observed sharp transition of grain boundary mobility with temperature and its dependence on bulk composition observed experimentally [640].

In contrast to the solute drag of the migrating boundary discussed above, only little is known about the reverse effect – the non-equilibrium segregation of solutes at

the moving grain boundaries, for example during recrystallisation and grain growth. This is despite the fact that the solute enrichment can be stronger than that of equilibrium segregation. For example, 1.6 times higher concentration of boron than its bulk concentration was detected on moving grain boundaries of an Fe–3mass.%Si alloy while no boron was found at static grain boundary [641]. Boron segregation is intensified with continuing recrystallization. If the velocity of the grain boundary migration decreases, boron grain boundary segregation also decreases and eventually disappears. The cause of these changes in the segregation behaviour is obviously the change of the width of the grain boundary during its migration. The broadening of the boundary results from its interaction with volume dislocations disappearing during grain boundary migration. The width  $\delta$  of the moving grain boundary can be expressed as

$$\delta = \delta_0 + v\tau\delta_\tau\Delta\rho, \quad (6.56)$$

where  $\delta_0$  is the width of the equilibrium grain boundary,  $v$  is the boundary velocity,  $\tau$  is the relaxation time for dislocation annihilation by moving grain boundary,  $\delta_\tau$  is the increment of the average width of unit area of the boundary during  $\tau$  and  $\Delta\rho$  is the difference of the dislocation density in deformed and new grains. The enrichment ratio of the solute at moving grain boundaries is then

$$\beta_I^\Phi = 1 + \frac{\delta}{v} \exp\left(\frac{U_0}{RT} - 1\right). \quad (6.57)$$

In (6.57),  $U_0$  is the potential of the solute atoms near the grain boundary. According to (6.56) and (6.57), the value  $\beta_B^\Phi = 1.7$  was determined for boron segregation at moving grain boundaries in an Fe–3mass.%Si alloy during its recrystallization at 1,273 K after 20% deformation [642].